THE JOURNAL OF PHYSICAL CHEMISTRY LETTERS
A JOURNAL OF THE AMERICAN CHEMICAL SOCIETY

pubs.acs.org/JPCL

Letter

Anisotropic Phonon Behavior and Phase Transition in Monolayer $ReSe_2$ Discovered by High Pressure Raman Scattering

Yuting Yan, Liyuan Chen, Kai Dai, Yafang Li, Lin Wang, Kai Jiang,* Anyang Cui, Jinzhong Zhang, and Zhigao Hu*

Cite This: J. Phys. Chem. Lett. 2023, 14, 7618−7625

Read Online

ACCESS | Metrics & More | Article Recommendations | Supporting Information

ABSTRACT: Re-based transition metal dichalcogenides have attracted extensive attention owing to their anisotropic structure and excellent properties in applications such as optoelectronic devices and electrocatalysis. The present study methodically investigated the evolution of specific Raman phonon mode behaviors and phase transitions in monolayer and bulk $ReSe_2$ under high pressure. Considering the distinctive anisotropic characteristics and the vibration vectors of Re and Se atoms exhibited by monolayer $ReSe_2$, we perform phonon dispersion calculations and propose a methodology utilizing pressure-dependent polarized Raman measurements to explore the precise structural evolution of monolayer $ReSe_2$ under the stress fields. Varied behaviors of the E_g-like and A_g-like modes, along with their specific vector transformations, have been identified in the pressure range 0−14.59 GPa. The present study aims to offer original perspectives on the physical evolution of Re-based transition metal dichalcogenides, elucidating their fundamental anisotropic properties and exploring potential applicability in diverse devices.

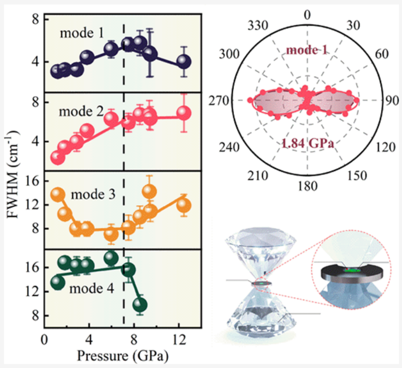

Recently, two-dimensional (2D) layered transition metal dichalcogenides (TMDs) with the component MX_2 (where M denotes a transition metal, such as Mo, Sn, W, Nb, and Hf, and X denotes a chalcogen such as S, Se, and Te) have attracted considerable attention due to their excellent optical properties and expansive prospects for practical applications.[1−3] Despite the general isotropic behavior observed in TMDs,[4] ReS_2 and $ReSe_2$ exhibit distinctive anisotropic characteristics attributed to their crystallization in a distorted $1T$ ($1T'$) diamond-chain structure with triclinic symmetry.[5−10] The low lattice symmetry of ReS_2 and $ReSe_2$ endows them with unique mechanical, electrical, optical, and thermal dynamical properties, which lead to their applicability to photodetectors,[11] electrochemical energy conversion,[12] polarization controllers, and related fields.[13,14] Moreover, monolayer $ReSe_2$ has a direct bandgap of approximately 1.22 eV,[15] which is narrower than that of most TMDs. The rare p-type conduction characteristics of $ReSe_2$ are highly desirable for photodetectors and electronic devices.[16] However, there has been limited research conducted on the internal physical structure of $ReSe_2$, which is crucial for practical applications. To enhance the properties of $ReSe_2$ devices and gain comprehensive insights into its physical structure, a thorough investigation into the lattice evolution and phase transition has become one of the imperative issues.

As we know, $1T'$ $ReSe_2$ is an ideal diamagnetic semiconductor that belongs to the transition-metal dichalcogenide family and has $P\bar{1}$ symmetry. It has been proposed that the evolution of its structure and properties has been observed through thermal field regulation and doping with other elements.[17] The stress field provides an alternative and effective avenue for regulating external fields, exerting influence on crystal structures by modifying chemical bonds and interatomic distances.[18] We created a sample chamber with a high-pressure environment using a diamond anvil cell (DAC), as depicted in Figure 1a. High pressure can be applied to modify the crystal structure of materials and mechanically adjust the lattice parameters of crystals, which has become a popular method for studying conventional superconductivity, interfacial coupling, and physical structure.[19,20] The investigation of the phase transition and structural evolution of $ReSe_2$ under high pressure is of paramount importance for enhancing its controllability and performance, creating new opportunities for its utilization in the fields of electronics, optoelectronics, and energy applications. Typically, low-symmetry arrangements transform into high-symmetry arrangements when it is subjected to high pressure, accompanied by the phase transition. In a previous pressure-dependent angular-dispersive X-ray diffraction (ADXRD) study, the phase transition pressure point of $ReSe_2$ was 9.98 GPa,[21] and the new phase above 10.5 GPa was identified as the $P\bar{1}'$ phase.[22] However, there is a scarcity of comprehensive

Received: June 30, 2023
Accepted: August 16, 2023

https://doi.org/10.1021/acs.jpclett.3c01784
J. Phys. Chem. Lett. 2023, 14, 7618−7625

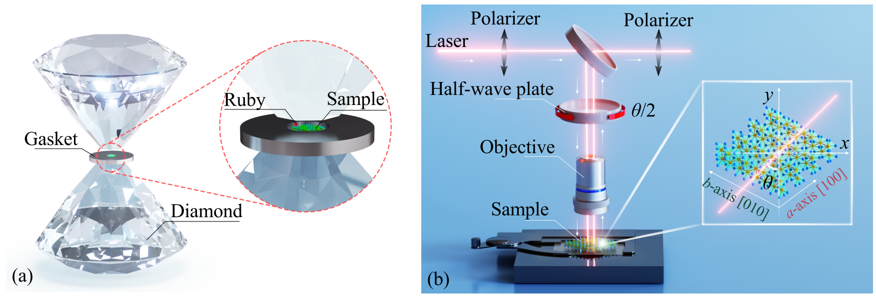

Figure 1. (a) Schematic diagram and optical graph demonstrate the specific structure of the diamond anvil cell (DAC) utilized for creating a high-pressure environment. The sample is placed within a small 120 μm diameter hole in a gasket. (b) Laser optical path, polarizers, objective, and half-wave plate for polarized Raman experiment. The enlarged view shows the anisotropic lattice feature of the top-view of monolayer $ReSe_2$ and the angle (θ) between the laser acquisition signal and the laboratory coordinate system. The direction of Re chains aligns with the b-axis [010].

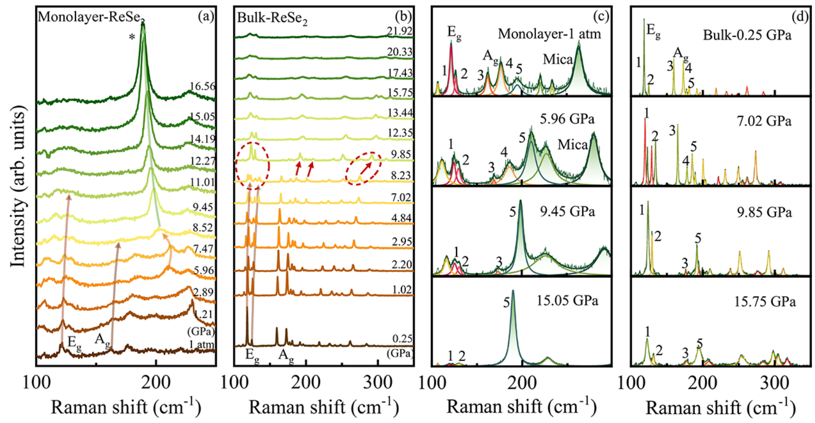

Figure 2. Representative pressure-dependent Raman spectra of (a) monolayer $ReSe_2$ and (b) bulk $ReSe_2$ from 1 atm to above 16.56 GPa. The dotted circles display the obvious Raman shifts among the pressure-dependent Raman measurements, while the overall trends of phonon modes are marked by arrows. (c, d) Lorentzian-shape deconvolution of Raman spectra at four selected pressures for monolayer $ReSe_2$ (1 atm and 5.96, 9.45, and 15.05 GPa) and bulk $ReSe_2$ (0.25, 7.02, 9.85, and 15.75 GPa), respectively. The phonon modes of E_g-like (1, 2), A_g-like (3, 4, 5), and mica are labeled.

studies concerning the phase transition and physical structure changes of monolayer $ReSe_2$ under the influence of stress fields. Fortunately, Raman scattering spectroscopy has been widely recognized as a nondestructive probe technique for studying various properties of 2D TMD semiconductors, including layer number, internal strain, and polarizability.[23−25] Thus, high-pressure Raman spectral measurements can be conducted to investigate the different phase transition pressure points and/or some new interesting phenomena.

Here, mica was selected as the substrate for our monolayer continuous films owing to its flatness, high thermal stability, low surface energy, and compatibility. We measured the Raman spectra of both monolayer and bulk $ReSe_2$ to investigate its phase transition and structure evolution. By examining the Raman intensity ratio between the E_g-like and A_g-like phonon modes, as well as analyzing the full width of half-maximum (FWHM), the critical pressure-dependent phase transition point can be ascertained. Additionally, the utilization of polarized Raman scattering enables the analysis of crystallinity, lattice symmetry, and molecular anisotropy, providing valuable insights into the anisotropic behavior of $ReSe_2$. As shown in Figure 1b, we employed different angle configurations for measurement polarization by rotating a half-wave plate and observed significant periodic variations (90° or 180°) in the intensity of distinct vibrational modes within monolayer $ReSe_2$. By analyzing the periodic variations in anisotropic Raman response and combining them with phonon dispersion calculations, the molecular vibrational directions corresponding to different phonon modes can be determined. The evolution of phonon modes accompanies the structural changes, prompting us to propose a methodology utilizing pressure-dependent polarized Raman measurements to explore the structural evolution of monolayer $ReSe_2$ under the influence of stress fields. Therefore, we subjected the system to a stress field and observed some discernible transitions in the periodic variation (from 180° to 90°) and alterations in the angle of maximum intensity in response to the applied stress field. Our discovery of pressure- and angle-dependent structural evolution provides novel perspectives and offers more possibilities for expanding applications of 2D TMD semiconductors.

High-pressure Raman spectroscopy measurements were performed to elucidate the pressure-dependent structure modulations. Figure 2a shows pressure-induced Raman spectra of monolayer $ReSe_2$ in the range of 0−15 GPa, respectively. At 0 GPa, the Raman spectrum of monolayer $ReSe_2$ exhibited major peaks around 121 cm^{-1} (E_g-like) and 163 cm^{-1} (A_g-like).[26−28] Due to the intricate lattice vibrations in monolayer $ReSe_2$, it becomes difficult to identify pure E_g or A_g modes corresponding to each Raman peak.[26] Therefore, we adopt E_g-like and A_g-like modes to describe the Raman phonon modes of $ReSe_2$. As the pressure increases, both E_g-like and A_g-like phonon modes shifted toward higher frequencies, while the intensity of all significant peaks decreased except for the signal

https://doi.org/10.1021/acs.jpclett.3c01784
J. Phys. Chem. Lett. 2023, 14, 7618−7625

from the mica substrate. Regarding the intensity enhancement observed around 200 cm^{-1} (*) in monolayer $ReSe_2$ under high pressure, we attribute it to the in-plane vibrations arising from the interaction of Re_4Se_8 unit cells within the *ab*-plane after the phase transition. For the bulk $ReSe_2$ shown in Figure 2b, several different phonon mode behaviors are apparent in the pressure range of 8.23−9.85 GPa, including the disappearance of weaker peaks in E_g-like modes, anomalous blueshift of some phonon modes, and a drastic decrease in the peaks located at 166 and 223 cm^{-1}. The pronounced shifts in the observed phonon modes can be primarily attributed to the altered lattice dynamics and phonon mode coupling resulting from the phase transition. Additionally, the anomalous behavior of certain phonon peaks may arise from the modified interatomic distances and bond angles in the lattice structure. We also measured pressure-dependent Raman spectra of the mica substrate to eliminate its interference (Supporting Information Figure S1). The results have demonstrated that a unit cell of $ReSe_2$ consists of 12 atoms and 18 Raman-active modes.[9,29] The main frequency range of Raman phonon modes from $ReSe_2$ is 100−300 cm^{-1}, corresponding to the dense spacing due to the low crystal symmetry of $ReSe_2$. Figure 2c,d reveals a Lorentzian-shaped decomposition for four selected pressures, allowing us to analyze the primary distinction of phonon modes as the pressure increased. Although only a few modes were observed in the monolayer $ReSe_2$ because of their weak intensities,[30] the E_g-like phonon mode (labeled as mode 1, 2) was observed at 121, 124 cm^{-1}, and the A_g-like phonon mode (labeled as mode 3, 4) was observed at 163, 174 cm^{-1}, respectively.

In order to uncover additional details in the variations of Raman spectra measurements, we extracted the phonon modes at different pressures (Supporting Information Figure S2). In the resistivity measurements of bulk $ReSe_2$ under different pressures, the critical point for the pressure-induced phase transition was determined to be 8.94 GPa (Supporting Information Figure S3), which is in agreement with the observations derived from the Raman spectroscopy measurements. The observed irregular variations in Raman modes and the change in resistance slope with increasing pressure can be attributed to the occurrence of a phase transition.[21] As indicated in Figure 3a, the intensity ratio of mode 1/mode 3

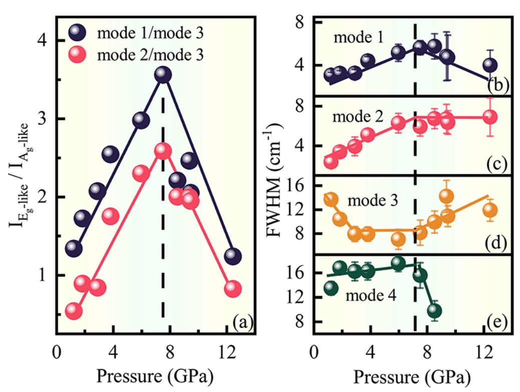

Figure 3. (a) The intensity ratios of the relative Raman phonon modes versus pressure are shown for monolayer $ReSe_2$. Purple balls represent the intensity ratio of mode 1/mode 3, while the ratio of mode 2/mode 3 is represented by pink balls. (b−e) Full width at half-maximum (FWHM) values of four Raman phonon modes (modes 1−4) with increasing the pressure.

and mode 2/mode 3 versus pressure can be used to precisely determine the competitive relationship between the E_g-like mode and A_g-like modes. The intensity ratio of the $P\bar{1}$ phase increased because of the higher sensitivity of the A_g-like phonon mode on pressure. Thus, the out-of-plane vibration modes were first affected when the pressure was applied to monolayer $ReSe_2$. However, when the pressure exceeded 7.50 GPa, the ratio decreased and approached 1 beyond 12 GPa. The intensities of E_g-like modes also rapidly decreased beyond 7.50 GPa, probably because of the evolution of the in-plane vibration structure after the phase transition. Therefore, in addition to the fact that out-of-plane vibration can be affected by pressure before in-plane vibration, the abrupt torsion of the intensity ratio for both mode 1/mode 3 and mode 2/mode 3 also supports the observation that the phase transition point is around 7.50 GPa. Similarly, as shown in Figure 3b−d, the FWHMs also exhibited sharp changes near the phase transition point.

Low lattice symmetry results in a relatively large unit cell of $ReSe_2$, consisting of four Re atoms and eight Se atoms (Supporting Information Figure S4). The existence of Re chains composed of quasi-one-dimensional Re_4 diamond-like clusters is the most distinct feature of monolayer $ReSe_2$ as an anisotropic material.[31,32] The Re chains align along the *b*-axis [010] of 1*T*' $ReSe_2$, which is nonorthogonal to the *a*-axis [100], with an approximate angle of 120°. Adjacent Re_4 diamond-like clusters on the *b*-axis are slightly larger than those on the *a*-axis.[33] Due to the relative complexity of the unit cell structure, distinguishing pure E_g-like and A_g-like mode vibrations from the corresponding Raman signals is challenging. Since $ReSe_2$ is an anisotropic material, angle-dependent absorption and lattice vibration can be represented using Raman tensors.[34] Therefore, the original Raman tensors (**R**) can be expressed as follows:

$$\mathbf{R} = \begin{pmatrix} a & d & e \\ d & b & f \\ e & f & c \end{pmatrix} \quad (1)$$

and the two-dimensional vectors of A_g phonon modes were[35]

$$\mathbf{R}(A_g) = \begin{pmatrix} |a|e^{i\phi_a} & & \\ & |b|e^{i\phi_b} & \\ & & |c|e^{i\phi_c} \end{pmatrix} \quad (2)$$

Quantitative analysis of angle-dependent Raman intensities can be conducted using the incident and scattered unitary vectors $\hat{e}_i$ and $\hat{e}_s$.[36] The Raman tensor can be used to express the Raman intensity as follows:[37,38]

$$I \propto |\hat{e}_s \cdot R \cdot \hat{e}_i|^2 \quad (3)$$

The vector

$$\hat{e}_i = (\cos\theta \ \ \sin\theta \ \ 0)$$

corresponds to the incident light, while

$$\hat{e}_i = \hat{e}_s = (\cos\theta \ \ \sin\theta \ \ 0)$$

is for the parallel configuration of the scattered light. Hence the intensity can be written as

https://doi.org/10.1021/acs.jpclett.3c01784
J. Phys. Chem. Lett. 2023, 14, 7618−7625

$$I(A_g) \propto |a|^2 \cos^4\theta + |b|^2 \sin^4\theta + 2|a||b| \cos(\phi_a - \phi_b) \cos^2\theta \sin^2\theta \tag{4}$$

and θ represents the angle between the y-axis of the laboratory coordinate system.

Considering the details of Raman phonon modes in the monolayer-$ReSe_2$ structure, we calculated the phonon dispersion (Supporting Information Figure S5) and identified 36 phonon vibration modes.[29−31] Using $\Gamma = 18(A_g + A_u)$, we determined the frequencies of E_g-like (modes 1 and 2) and A_g-like (modes 3 and 4) modes from the phonon dispersion to be 117.9, 121.5, 158.5, and 174.6 cm^{-1}, respectively. The vibration vectors for each of the 12 atoms in a unit cell were extracted, with the calculation of its components along the b-axis:

$$b_n = \nu_{b_n} + \nu_{a_n} \cos\gamma + \nu_{c_n} \cos\alpha \tag{5}$$

for atom ordinal n = 1, 2, 3, ..., 12, $\gamma = 118.8°$, $\alpha = 104.4°$. γ represents the angle between the a and b axes of the unit cell, while γ denotes the angle between the b and c axes. Owing to the situation where two atoms (Re_{2i-1} and Re_{2i} (i = 1, 2) or Se_{2j-1} and Se_{2j} (j = 1, 2, 3, 4)) are stretched along the b-axis in opposition, if we want to obtain the total vibration intensity along the b-axis, all the vectors have to be taken in absolute value:

$$b = \sum_{n=1}^{12} |b_n| \tag{6}$$

Similarly, the vibration intensity along the a-axis can be expressed as

$$a_n = \nu_{a_n} + \nu_{b_n} \cos\gamma + \nu_{c_n} \cos\beta \tag{7}$$

while $\beta = 91.96°$, with

$$a = \sum_{n=1}^{12} |a_n| \tag{8}$$

Therefore, we calculated the phonon dispersion of monolayer $ReSe_2$ in four selected pressures (Supporting Information Figure S5). As presented in Table 1, the values of a and b for four phonon modes at 0, 3.89, and 5.35 GPa were extracted. We held the γ angle of the unit cell fixed and achieved the variations by compressing the bond lengths within the lattice structure when calculating the phonon dispersion at different pressures. Subsequently, the values of a and b are inserted into the lattice coordinate system to obtain the angle (θ) of the vibrational direction relative to the counterclockwise direction of the b-axis. According to the trigonometric formula,

$$r^2 = a^2 + b^2 - 2ab\cos\gamma \tag{9}$$

$$\theta = \arcsin\frac{b \sin\gamma}{r} \tag{10}$$

from which we can deduce the angle between two phonon modes. Table 1 displays the maximum angle between the E_g-like and A_g-like modes at 0 GPa, which is 13.73°. As the pressure increases, both modes undergo counterclockwise rotation, with the E_g-like mode rotating rapidly before 3.89 GPa. The E_g-like and A_g-like phonon modes were at approximately the same angle after 5.35 GPa. In addition, all phonon modes experience a blueshift trend.

The correspondence between Raman phonon modes and specific molecular vibrations has not been clarified in pressure-dependent Raman spectra experiments. The polarized Raman scattering technique (see Figure 1 and Supporting Information Figure S6) is a practical method for determining molecular symmetry. The Raman-active modes of $ReSe_2$ can be expressed as $\Gamma_{\text{Raman-active}} = 18A_g$. Although all modes are formally A_g phonon modes, multiple discrepancies are observed between polarized scattering signals.[39] In our experiment, the laser collected the Raman signal along the z direction of the laboratory coordinate system, limiting us to obtain information in the xy-plane of the monolayer $ReSe_2$. During the compression process, the mica substrate confines the in-plane stretching vibration of $ReSe_2$. Therefore, the effect of pressure on stretching vibrations is mainly reflected in the c-axis direction and bending vibrations in the ab-plane, achieved by altering the distances and bond angles between atoms in the crystal structure of $ReSe_2$.

To ensure accurate measurements, it is necessary to identify the crystal orientation of monolayer $ReSe_2$ in the DAC, which can be challenging due to uncertainty in the sample installation direction. Previous studies have reported that the vibrations along the b-axis direction are associated with the A_g-like mode located at 163 cm^{-1} (mode 3) and 174 cm^{-1} (mode 4).[9,26] Additionally, our calculated phonon dispersion study of monolayer $ReSe_2$ (Table 1) also showed that the A_g-like mode at 174.6 cm^{-1} had the minimum angle with respect to the b-axis. Therefore, by analyzing the polarization characteristics of modes 3 and 4 at minimum pressure (1.84 GPa), we identified the directions of mode 3 and the b-axis as 103.83° and 128.01°, as shown in Figure 4 and Supporting Information Figure S7. The solid lines represent the outcomes of Lorenzian fitting, facilitating the derivation of functional relationships between the Raman intensity and the angle for each phonon mode. Nevertheless, before this analysis, the intensity values for the phonon modes were acquired through Lorenzian fitting applied to the raw Raman spectra. The maximum intensity angle corresponding to mode 1 was 92.75°, approximately 11.08° counterclockwise from mode 3, while the angle difference between two phonon modes in the calculated phonon dispersion was 13.73°. This consistency between the results validated the accuracy of the proposed experimental method. As the pressure increases, mode 3 exhibits a counterclockwise rotation trend from 103.83° to 54.36°,

Table 1. Frequencies and the Angle (θ) between the b-Axis of Four Phonon Modes Were Calculated through Phonon Dispersion Calculations at 0, 3.89, and 5.35 GPa

pressure (GPa)	vibration	mode	frequency (cm^{-1})	a	b	θ (deg)
0	E_g-like	mode 1	117.9	3.5	2.6	35.4
0	E_g-like	mode 2	121.5	1.8	1.2	37.3
0	A_g-like	mode 3	158.5	1.6	2.4	24.2
0	A_g-like	mode 4	174.6	2.0	3.2	23.5
3.89	E_g-like	mode 1	123.1	3.6	2.8	70.5
3.89	E_g-like	mode 2	128.4	1.8	1.3	74.4
3.89	A_g-like	mode 3	164.8	1.3	1.4	56.2
3.89	A_g-like	mode 4	180.5	2.1	2.5	51.3
5.35	E_g-like	mode 1	128.9	2.3	1.8	71.1
5.35	A_g-like	mode 3	166.4	1.1	0.9	70.9
5.35	A_g-like	mode 4	177.9	1.7	1.2	76.3

https://doi.org/10.1021/acs.jpclett.3c01784
J. Phys. Chem. Lett. 2023, 14, 7618−7625

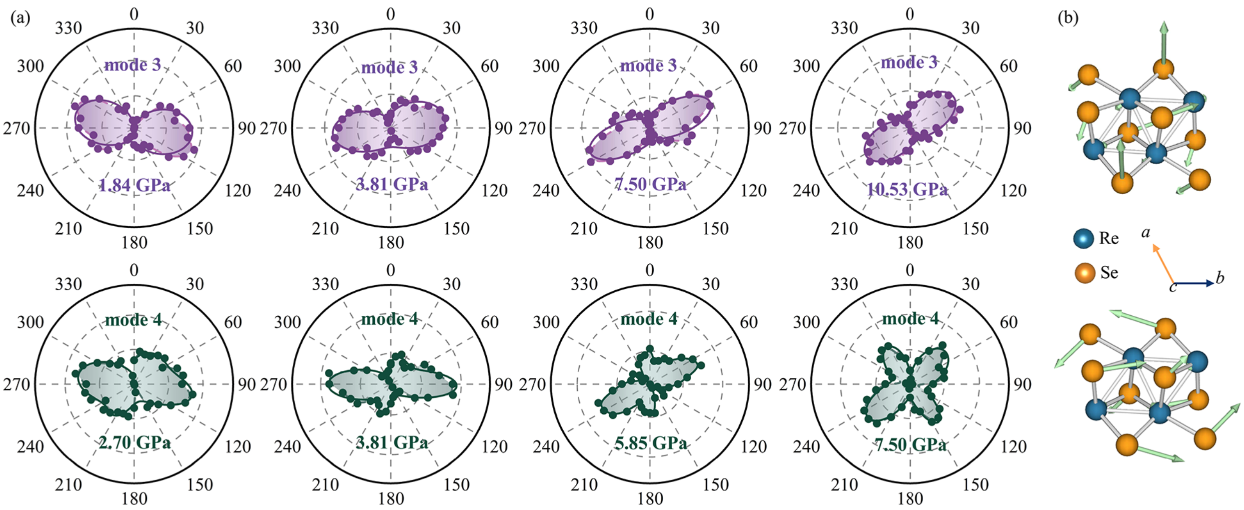

Figure 4. (a) Representative angle-dependent Raman intensity of mode 3 (purple circles) and mode 4 (green circles) from 0 to 10.53 GPa. (b) Specific schematic diagram of A_g-like phonon vibration vectors.

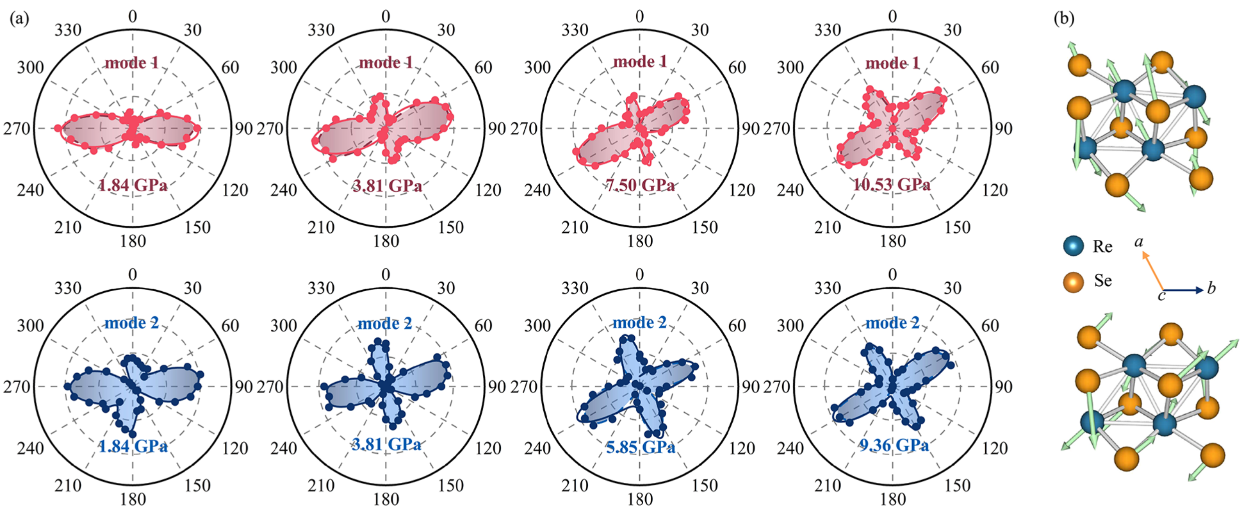

Figure 5. (a) Pressure-dependent anisotropic Raman intensity of mode 1 (pink circles) and mode 2 (blue circles) in the pressure range of 0−10.53 GPa. (b) Schematic vibration vectors of the E_g-like phonon mode in the unit cell, which is obtained by theoretical calculation.

while mode 4 moves from 102.21° to 45.62°, respectively. The rotational angle amplitudes of the two phonon modes at various pressures and their difference at the same pressure point conform well to the theoretical calculations. When the pressure exceeded 7.50 GPa, the counterclockwise rotation weakened considerably and ultimately stabilized. The observations suggest that the bonding angles of $ReSe_2$ exhibit limited responsiveness to applied pressure, following the occurrence of a phase transition. As illustrated in Figure 5 and Supporting Information Figure S8, mode 1 exhibited counterclockwise rotation from 92.75° to 56.53°, whereas mode 2 depicted a similar rotation from 85.32° to 59.14°, respectively.

In the analysis of the calculated phonon dispersion, we observed that the vibrational intensity of modes 1 and 2 remained relatively constant within the pressure range of 0−3.89 GPa, with noticeable variations primarily in the orientation of the vibrational vector. By contrast, modes 3 and 4 not only underwent rotations but also decreased in intensity during the compression. These modes are associated with the direction of the Re chains, and their rotation ceases as the pressure increases and $ReSe_2$ undergoes a phase transition to the $P\overline{1}'$ phase. Following the phase transition, the Re chains persist; however, they experience lattice distortion and an increase in the angle with respect to the *c*-axis due to compression. According to our experimental and theoretical findings, the in-plane vibrational modes parallel to the *ab*-plane experienced a predominant angular distortion, while the out-of-plane vibrational modes suffered substantial intensity loss during the compression. The pressure-dependent experiments on bulk $ReSe_2$ excluded the possibility that the reduction in the out-of-plane vibration intensity in the *ab*-plane is caused by rotation toward the *z*-axis of the laboratory coordinate system. With the continued increase of pressure after the phase transition point, both in-plane and out-of-plane vibrational modes stopped rotating and displayed only intensity changes. After the phase transition, a structurally enhanced symmetry becomes evident, leading to a stronger tendency for structural compression rather than structural distortion under further stress field application. Upon transitioning to the $P\overline{1}'$ phase, the compressibility along the *c*-axis is similar to that along the *a*-axis, allowing the compressibility along the *b*-axis (Re chain)

https://doi.org/10.1021/acs.jpclett.3c01784
J. Phys. Chem. Lett. 2023, 14, 7618−7625

to be employed in analyzing the competition between in-plane and out-of-plane vibrations. Under ideal hydrostatic pressure, the compression along the *b*-axis is inevitable. Consequently, in comparison to out-of-plane vibrations, the in-plane vibrations exhibit a higher sensitivity to pressure after the phase transition. The lattice structure demonstrates increased stability, with the primary alterations remaining confined to the crystal axis lengths unless subjected to more extreme stress fields. In conclusion, the present study provides valuable insights into the vibrational behavior of monolayer $ReSe_2$ under high pressure, thereby contributing to a deeper understanding of its lattice dynamics in stress fields.

In conclusion, this study comprehensively investigated the pressure-dependent and anisotropic phonon behaviors of monolayer $ReSe_2$. We identified the phase transition pressure points for the monolayer and bulk $ReSe_2$ at 7.50 and 8.23 GPa, respectively. By comparing the intensities of E_g-like and A_g-like phonon modes, we discovered that A_g-like phonon modes were more sensitive to the stress field, while the E_g-like mode became dominant near 7.50 GPa. By performing polarized Raman measurements and phonon dispersion studies, we successfully determined the orientation of the crystallographic axis in the diamond anvil cell (DAC). Furthermore, we put forward a methodology employing pressure-dependent polarized Raman measurements to investigate the intricate structural evolution of monolayer $ReSe_2$ under the influence of stress fields, thereby providing valuable insights into its dynamic behavior under high pressure conditions. The anisotropic Raman spectroscopy revealed the variation of the phonon modes and their corresponding molecular structures under high-pressure environments and analyzed the difference of sensitivity to stress field due to the change of structural symmetry before and after the phase transition. This work will be advantageous to in-depth physical structure research on anisotropic 2D TMDs and will provide basic theoretical support for ameliorating the device properties.

■ METHODS

Sample Preparation. The monolayer $ReSe_2$ was grown using the chemical vapor deposition (CVD) method in a three-zone horizontal tube furnace. Several sapphire pieces were placed in the high-temperature zone of the tube (550 °C), while the precursor material Re_2O_7 was positioned in the middle-temperature zone (340 °C) and Se particles were located in the edge-temperature zone. Growth carrier gases consisting of 100 sccm of argon (Ar) and 10 sccm of hydrogen (H_2) were employed. The growth process was carried out under a pressure of 3000 Pa for a duration of 10 min. The samples were naturally cooled to room temperature in the furnace after the growth. The monolayer $ReSe_2$ films were first grown on a sapphire substrate and subsequently were transferred to a mica substrate with the aid of a 2D-material directional transfer auxiliary platform.

Pressure-Dependent Polarized Raman Scattering Measurements. Raman scattering measurements were recorded by using a Jobin-Yvon LabRAM HR Evolution spectrometer. As illustrated in Figure 1a, a Mao-Bell-type diamond anvil cell (DAC) equipped with a stainless steel gasket and two 300 μm culet diamonds was applied to create a high-pressure environment. The silicone oil acted as a pressure-transmitting medium (PTM) to transfer pressure. The $ReSe_2$ film with a thinned down mica substrate was carefully separated into a plane smaller than that of the gasket's aperture and subsequently transferred onto to the DAC by a sharp tweezer. A laser with the wavelength of 633 nm served as excitation sources, and a 1800 grooves/mm grating was used to take the scattering information. A 50× objective was employed to focus the laser. The pressure value was calibrated by the ruby luminescence method. The polarizer and analyzer were placed in the excitation and detection paths, respectively. A rotatable half-wave plate with a phase retardation of $\lambda/2$ was positioned above the objective to adjust the incident light angle, as depicted in Figure 1b. Information about the sample at different angles was obtained by rotating the half-wave plate.

Phonon Dispersion and DFT Calculations. The projector-augmented wave (PAW) method was used to describe ion−electron interaction, while the density functional theory (DFT) calculations were performed in the Vienna *ab initio* simulation package (VASP). The exchange−correlation functional was approximated using the generalized gradient approximation (GGA) of Perdew−Burke−Erzerhof (PBE).[40] The unit cell of the $1T'$-phase structure, consisting of four formula units, was adopted. The unit cell of the $1T'$ phase structure, consisting of four formula units, was adopted. All reported energies are given in units of eV/f.u. For structural optimization, the convergence threshold was established at $1.0 \times 1 \text{ x } 10^{-6}$ for energy and 0.01 eV/Å for force. A 15 × 15 × 1 Monkhorst−Pack k-point mesh was used to sample the Brillouin zone. The harmonic approximation, as implemented in the PHONOPY package, was utilized to determine the vibrational energy and entropy. Vibrational frequencies were derived from the force constant matrix of fully relaxed geometries. To ensure the accuracy of periodic boundary conditions, a vacuum layer with a thickness of 20 Å along the *c*-axis was introduced.

■ ASSOCIATED CONTENT

Supporting Information

The Supporting Information is available free of charge at https://pubs.acs.org/doi/10.1021/acs.jpclett.3c01784.

> Pressure-dependent Raman phonon modes variation of monolayer, bulk $ReSe_2$, and mica; phonon modes variation of monolayer and bulk $ReSe_2$; pressure-dependent resistance of bulk $ReSe_2$; molecular structure schematic diagram of the monolayer $ReSe_2$; calculated phonon dispersion in four selected pressures; optical path flow diagram in pressure- and angle-dependent Raman measurements; anisotropic Raman response of modes 3 and 4; polarized Raman intensity of modes 1 and 2 (PDF)

■ AUTHOR INFORMATION

Corresponding Authors

Kai Jiang − *Technical Center for Multifunctional Magneto-Optical Spectroscopy (Shanghai), Engineering Research Center of Nanophotonics & Advanced Instrument (Ministry of Education), Department of Physics, School of Physics and Electronic Science, East China Normal University, Shanghai 200241, China; School of Arts and Sciences, Shanghai Dianji University, Shanghai 200240, China*; Email: kjiang@ee.ecnu.edu.cn

Zhigao Hu − *Technical Center for Multifunctional Magneto-Optical Spectroscopy (Shanghai), Engineering Research Center of Nanophotonics & Advanced Instrument (Ministry of Education), Department of Physics, School of Physics and Electronic Science, East China Normal University, Shanghai*

200241, China; School of Arts and Sciences, Shanghai Dianji University, Shanghai 200240, China; Collaborative Innovation Center of Extreme Optics, Shanxi University, Taiyuan, Shanxi 030006, China; orcid.org/0000-0003-0575-2191; Phone: +86-21-54345150; Email: zghu@ee.ecnu.edu.cn; Fax: +86-21-54342933

Authors

Yuting Yan — *Technical Center for Multifunctional Magneto-Optical Spectroscopy (Shanghai), Engineering Research Center of Nanophotonics & Advanced Instrument (Ministry of Education), Department of Physics, School of Physics and Electronic Science, East China Normal University, Shanghai 200241, China*

Liyuan Chen — *Technical Center for Multifunctional Magneto-Optical Spectroscopy (Shanghai), Engineering Research Center of Nanophotonics & Advanced Instrument (Ministry of Education), Department of Physics, School of Physics and Electronic Science, East China Normal University, Shanghai 200241, China*

Kai Dai — *Technical Center for Multifunctional Magneto-Optical Spectroscopy (Shanghai), Engineering Research Center of Nanophotonics & Advanced Instrument (Ministry of Education), Department of Physics, School of Physics and Electronic Science, East China Normal University, Shanghai 200241, China*

Yafang Li — *Technical Center for Multifunctional Magneto-Optical Spectroscopy (Shanghai), Engineering Research Center of Nanophotonics & Advanced Instrument (Ministry of Education), Department of Physics, School of Physics and Electronic Science, East China Normal University, Shanghai 200241, China*

Lin Wang — *Technical Center for Multifunctional Magneto-Optical Spectroscopy (Shanghai), Engineering Research Center of Nanophotonics & Advanced Instrument (Ministry of Education), Department of Physics, School of Physics and Electronic Science, East China Normal University, Shanghai 200241, China*

Anyang Cui — *Technical Center for Multifunctional Magneto-Optical Spectroscopy (Shanghai), Engineering Research Center of Nanophotonics & Advanced Instrument (Ministry of Education), Department of Physics, School of Physics and Electronic Science, East China Normal University, Shanghai 200241, China; Key Laboratory of Optoelectronic Material and Device, Department of Physics, Shanghai Normal University, Shanghai 200234, China; Chongqing Key Laboratory of Precision Optics, Chongqing Institute of East China Normal University, Chongqing 401120, China;* orcid.org/0000-0002-2517-8871

Jinzhong Zhang — *Technical Center for Multifunctional Magneto-Optical Spectroscopy (Shanghai), Engineering Research Center of Nanophotonics & Advanced Instrument (Ministry of Education), Department of Physics, School of Physics and Electronic Science, East China Normal University, Shanghai 200241, China;* orcid.org/0000-0003-1511-4281

Complete contact information is available at: https://pubs.acs.org/10.1021/acs.jpclett.3c01784

Author Contributions

Y. Yan initiated and designed the experiments and wrote the manuscript. L. Chen initiated and performed the calculations. Y. Yan, K. Dai, Y. Li, K. Jiang, A. Cui, and Z. Hu had sufficient discussions about Raman data. K. Jiang, J. Zhang, and Z. Hu discussed the underlying mechanism. L. Wang provided the resistance measurements. All of the authors contributed to the manuscript preparation.

Notes

The authors declare no competing financial interest.

■ ACKNOWLEDGMENTS

The authors are grateful to Drs. Ziyou Zhang and Hongliang Dong from Center for High Pressure Science and Technology Advanced Research, Shanghai, for the experimental assistance. This work was financially supported by the National Natural Science Foundation of China (Grants 62090013, 61974043, 12104156, and 62074058), National Key Research and Development Program of China (Grant 2019YFB2203403), Projects of Science and Technology Commission of Shanghai Municipality (Grant 21JC1402100), Natural Science Foundation of Chongqing, China (Grant CSTB2022NSCQ-MSX1367), and the Program for Professor of Special Appointment (Eastern Scholar) at Shanghai Institutions of Higher Learning.

■ REFERENCES

(1) Wang, Q. H.; Kalantar-Zadeh, K.; Kis, A.; Coleman, J. N.; Strano, M. S. Electronics and optoelectronics of two-dimensional transition metal dichalcogenides. *Nat. Nanotechnol.* **2012**, *7*, 699−712.

(2) Ying, J. J.; Paudyal, H.; Heil, C.; Chen, X. J.; Struzhkin, V. V.; Margine, E. R. Unusual Pressure-Induced Periodic Lattice Distortion in $SnSe_2$. *Phys. Rev. Lett.* **2018**, *121*, 027003.

(3) Ran, J. R.; Chen, L.; Wang, D. Y.; Talebian-Kiakalaieh, A.; Jiao, Y.; Adel Hamza, M.; Qu, Y.; Jing, L. Q.; Davey, K.; Qiao, S. Z. Atomic-Level Regulated 2D $ReSe_2$: A Universal Platform Boostin Photocatalysis. *Adv. Mater.* **2023**, *35*, 2210164.

(4) Chhowalla, M.; Shin, H. S.; Eda, G.; Li, L. J.; Loh, K. P.; Zhang, H. The chemistry of two-dimensional layered transition metal dichalcogenide nanosheets. *Nat. Chem.* **2013**, *5*, 263−275.

(5) Lamfers, H.-J.; Meetsma, A.; Wiegers, G. A.; de Boer, J. L. The crystal structure of some rhenium and technetium dichalcogenides. *J. Alloys Compd.* **1996**, *241*, 34−39.

(6) Chenet, D. A.; Aslan, B.; Huang, P. Y.; Fan, C.; van der Zande, A. M.; Heinz, T. F.; Hone, J. C. In-Plane Anisotropy in Mono- and Few-Layer ReS_2 Probed by Raman Spectroscopy and Scanning Transmission Electron Microscopy. *Nano Lett.* **2015**, *15*, 5667−5672.

(7) He, R.; Yan, J. A.; Yin, Z. Y.; Ye, Z. P.; Ye, G. H.; Cheng, J.; Li, J.; Lui, C. H. Coupling and Stacking Order of ReS_2 Atomic Layers Revealed by Ultralow-Frequency Raman Spectroscopy. *Nano Lett.* **2016**, *16*, 1404−1409.

(8) Kipczak, Ł.; Grzeszczyk, M.; Olkowska-Pucko, K.; Babiński, A.; Molas, M. R. The optical signature of few-layer $ReSe_2$. *J. Appl. Phys.* **2020**, *128*, 044302.

(9) Choi, Y.; Kim, K.; Lim, S. Y.; Kim, J.; Park, J. M.; Kim, J. H.; Lee, Z.; Cheong, H. Complete determination of the crystallographic orientation of ReX_2 (X=S, Se) by polarized Raman spectroscopy. *Nanoscale Horiz* **2020**, *5*, 308−315.

(10) Fang, Y. Q.; Lv, X. M.; Lv, Z. R.; Wang, Y.; Zheng, G. F.; Huang, F. Q. Electron-Extraction Engineering Induced 1*T*″-1*T*′ Phase Transition of $Re_{0.75}V_{0.25}Se_2$ for Ultrafast Sodium Ion Storage. *Adv. Sci.* **2022**, *9*, 2205680.

(11) Zhang, E. Z.; Wang, P.; Li, Z.; Wang, H. F.; Song, C. Y.; Huang, C.; Chen, Z. G.; Yang, L.; Zhang, K. T.; Lu, S. H.; Wang, W. Y.; Liu, S. S.; Fang, H. H.; Zhou, X. H.; Yan, H. G.; Zou, J.; Wan, X. G.; Zhou, P.; Hu, W. D.; Xiu, F. X. Tunable Ambipolar Polarization-Sensitive Photodetectors Based on High-Anisotropy $ReSe_2$ Nanosheets. *ACS Nano* **2016**, *10*, 8067−8077.

(12) Zhuang, M. H.; Xu, G.-L.; Gan, L.-Y.; Dou, Y. B.; Sun, C.-J.; Ou, X. W.; Xie, Y. Y.; Liu, Z. J.; Cai, Y. T.; Ding, Y.; Abidi, I. H.;

Tyagi, A.; Amine, K.; Luo, Z. T. Sub-5nm edge-rich 1*T*-$ReSe_2$ as bifunctional materials for hydrogen evolution and sodium-ion storage. *Nano Energy* **2019**, *58*, 660−668.
(13) Zhong, H.-X.; Gao, S. Y.; Shi, J.-J.; Yang, L. Quasiparticle band gaps, excitonic effects, and anisotropic optical properties of the monolayer distorted 1*T* diamond-chain structures ReS_2 and $ReSe_2$. *Phys. Rev. B* **2015**, *92*, 115438.
(14) Volckaert, K.; Choi, B. K.; Kim, H. J.; Biswas, D.; Puntel, D.; Peli, S.; Parmigiani, F.; Cilento, F.; Chang, Y. J.; Ulstrup, S. External screening and lifetime of exciton population in single-layer $ReSe_2$ probed by time- and angle-resolved photoemission spectroscopy. *Phys. Rev. Mater.* **2023**, *7*, L041001.
(15) Arora, A.; Noky, J.; Drüppel, M.; Jariwala, B.; Deilmann, T.; Schneider, R.; Schmidt, R.; Del Pozo-Zamudio, O.; Stiehm, T.; Bhattacharya, A.; Krüger, P.; Michaelis de Vasconcellos, S.; Rohlfing, M.; Bratschitsch, R. Highly Anisotropic in-Plane Excitons in Atomically Thin and Bulklike 1*T*'-$ReSe_2$. *Nano Lett.* **2017**, *17*, 3202−3207.
(16) Cui, F. F.; Li, X. B.; Feng, Q. L.; Yin, J. B.; Zhou, L.; Liu, D. Y.; Liu, K. Q.; He, X. X.; Liang, X.; Liu, S. Z.; Lei, Z. B.; Liu, Z. H.; Peng, H. L.; Zhang, J.; Kong, J.; Xu, H. Epitaxial growth of large-area and highly crystalline anisotropic $ReSe_2$ atomic layer. *Nano Res.* **2017**, *10*, 2732−2742.
(17) Jiang, S. L.; Zhao, L. Y.; Shi, Y. P.; Xie, C. Y.; Zhang, N.; Zhang, Z. P.; Huan, Y. H.; Yang, P. F.; Hong, M.; Zhou, X. B.; Shi, J. P.; Zhang, Q.; Zhang, Y. F. Temperature-dependent Raman spectroscopy studies of the interface coupling effect of monolayer $ReSe_2$ single crystals on Au foils. *Nanotechnology* **2018**, *29*, 204003.
(18) Yan, Y. T.; Cui, A. Y.; Dai, K.; Ye, Y.; Jiang, K.; Zhang, J. Z.; Feng, J. J.; Dong, H. L.; Hu, Z. G. Pressure- and Temperature-Induced Structural Phase Diagram of Lead-Free $K_{0.5}Na_{0.5}NbO_3$-0.05$LiNbO_3$ Single Crystals: Raman Scattering and Infrared Study. *ACS Appl. Mater. Interfaces* **2022**, *14*, 45590−45599.
(19) Drozdov, A. P.; Eremets, M. I.; Troyan, I. A.; Ksenofontov, V.; Shylin, S. I. Conventional superconductivity at 203 kelvin at high pressures in the sulfur hydride system. *Nature* **2015**, *525*, 73−76.
(20) Chen, Y. B.; Ke, F.; Ci, P. H.; Ko, C.; Park, T.; Saremi, S.; Liu, H. L.; Lee, Y.; Suh, J.; Martin, L. W.; Ager, J. W.; Chen, B.; Wu, J. Q. Pressurizing Field-Effect Transistors of Few-Layer MoS_2 in a Diamond Anvil Cell. *Nano Lett.* **2017**, *17*, 194−199.
(21) Kao, Y. C.; Huang, T.; Lin, D. Y.; Huang, Y. S.; Tiong, K. K.; Lee, H. Y.; Lin, J. M.; Sheu, H. S.; Lin, C. M. Anomalous structural phase transition properties in $ReSe_2$ and Au-doped $ReSe_2$. *J. Chem. Phys.* **2012**, *137*, 024509.
(22) Zhang, J. R.; Sun, E. M.; Feng, X. L.; Liu, H. Y.; Redfern, S. A. T.; Kanchana, V.; Liu, G. T.; Wang, H. B. Phase transition and superconductivity in ReS_2, $ReSe_2$ and $ReTe_2$. *Phys. Chem. Chem. Phys.* **2018**, *20*, 29472−29479.
(23) Li, Y. F.; Dai, K.; Gao, L. C.; Zhang, J. Z.; Cui, A. Y.; Jiang, K.; Li, Y. W.; Shang, L. Y.; Zhu, L. Q.; Hu, Z. G. Tunable lattice dynamics and dielectric functions of two-dimensional Bi_2O_2Se: striking layer and temperature dependent effects. *Nanoscale* **2023**, *15*, 2323−2331.
(24) Cui, A. Y.; Cao, X. H.; Ye, Y.; Jiang, K.; Zhu, L. Q.; Jiang, M. H.; Rao, G. H.; Li, Y. W.; Hu, Z. G.; Chu, J. H. Phase transitions and phonon thermodynamics in giant piezoelectric Mn-doped $K_{0.5}Na_{0.5}NbO_3$-$LiBiO_3$ crystals studied by Raman spectroscopy. *Phys. Rev. B* **2020**, *102*, 214102.
(25) Jiang, K.; Cui, A. Y.; Shao, S.; Feng, J. J.; Dong, H. L.; Chen, B.; Wang, Y. C.; Hu, Z. G.; Chu, J. H. New Pressure Stabilization Structure in Two-Dimensional $PtSe_2$. *J. Phys. Chem. Lett.* **2020**, *11*, 7342−7349.
(26) Zhao, H.; Wu, J. B.; Zhong, H. X.; Guo, Q. S.; Wang, X. M.; Xia, F. N.; Yang, L.; Tan, P. H.; Wang, H. Interlayer interactions in anisotropic atomically thin rhenium diselenide. *Nano Res.* **2015**, *8*, 3651−3661.
(27) Hafeez, M.; Gan, L.; Li, H. Q.; Ma, Y.; Zhai, T. Y. Chemical Vapor Deposition Synthesis of Ultrathin Hexagonal $ReSe_2$ Flakes for Anisotropic Raman Property and Optoelectronic Application. *Adv. Mater.* **2016**, *28*, 8296−8301.
(28) Jiang, S. L.; Zhang, Z. P.; Zhang, N.; Huan, Y. H.; Gong, Y.; Sun, M. X.; Shi, J. P.; Xie, C. Y.; Yang, P. F.; Fang, Q. Y.; Li, H.; Tong, L. M.; Xie, D.; Gu, L.; Liu, P.; Zhang, Y. F. Application of chemical vapor-deposited monolayer $ReSe_2$ in the electrocatalytic hydrogen evolution reaction. *Nano Res.* **2018**, *11*, 1787−1797.
(29) Wolverson, D.; Crampin, S.; Kazemi, A. S.; Ilie, A.; Bending, S. J. Raman Spectra of Monolayer, Few-Layer, and Bulk $ReSe_2$: An Anisotropic Layered Semiconductor. *ACS Nano* **2014**, *8*, 11154−11164.
(30) Taube, A.; Łapinska, A.; Judek, J.; Zdrojek, M. Temperature dependence of Raman shifts in layered $ReSe_2$ and $SnSe_2$ semiconductor nanosheets. *Appl. Phys. Lett.* **2015**, *107*, 013105.
(31) Lorchat, E.; Froehlicher, G.; Berciaud, S. Splitting of Interlayer Shear Modes and Photon Energy Dependent Anisotropic Raman Response in N-Layer $ReSe_2$ and ReS_2. *ACS Nano* **2016**, *10*, 2752−2760.
(32) Hong, M.; Zhou, X. B.; Gao, N.; Jiang, S. L.; Xie, C. Y.; Zhao, L. Y.; Gao, Y.; Zhang, Z. P.; Yang, P. F.; Shi, Y. P.; Zhang, Q.; Liu, Z. F.; Zhao, J. J.; Zhang, Y. F. Identifying the Non-Identical Outermost Selenium Atoms and Invariable Band Gaps across the Grain Boundary of Anisotropic Rhenium Diselenide. *ACS Nano* **2018**, *12*, 10095−10103.
(33) Lin, Y. C.; Komsa, H. P.; Yeh, C. H.; Björkman, T.; Liang, Z. Y.; Ho, C. H.; Huang, Y. S.; Chiu, P. W.; Krasheninnikov, A. V.; Suenaga, K. Single-Layer ReS_2: Two-Dimensional Semiconductor with Tunable In-Plane Anisotropy. *ACS Nano* **2015**, *9*, 11249−11257.
(34) Ling, X.; Huang, S. X.; Hasdeo, E. H.; Liang, L. B.; Parkin, W. M.; Tatsumi, Y.; Nugraha, A. R.; Puretzky, A. A.; Das, P. M.; Sumpter, B. G.; Geohegan, D. B.; Kong, J.; Saito, R.; Drndic, M.; Meunier, V.; Dresselhaus, M. S. Anisotropic Electron-Photon and Electron-Phonon Interactions in Black Phosphorus. *Nano Lett.* **2016**, *16*, 2260−2267.
(35) Kim, M.; Han, S.; Kim, J. H.; Lee, J.-U.; Lee, Z.; Cheong, H. Determination of the thickness and orientation of few-layer tungsten ditelluride using polarized Raman spectroscopy. *2D Mater.* **2016**, *3*, 034004.
(36) Ribeiro, H. B.; Pimenta, M. A.; De Matos, C. J. S.; Moreira, R. L.; Rodin, A. S.; Zapata, J. D.; De Souza, E. A. T.; Castro Neto, A. H. Unusual Angular Dependence of the Raman Response in Black Phosphorus. *ACS Nano* **2015**, *9*, 4270−4276.
(37) Kranert, C.; Sturm, C.; Schmidt-Grund, R.; Grundmann, M. Raman Tensor Formalism for Optically Anisotropic Crystals. *Phys. Rev. Lett.* **2016**, *116*, 127401.
(38) Ding, Y.; Zheng, W.; Lu, X. F.; Liang, Y. L.; Zhu, Y. M.; Jin, M. G.; Huang, F. Raman Tensor of Layered SnS_2. *J. Phys. Chem. Lett.* **2020**, *11*, 10094−10099.
(39) Hart, L.; Dale, S.; Hoye, S.; Webb, J. L.; Wolverson, D. Rhenium Dichalcogenides: Layered Semiconductors with Two Vertical Orientations. *Nano Lett.* **2016**, *16*, 1381−1386.
(40) Tang, Q. Tuning the phase stability of Mo-based TMD monolayers through coupled vacancy defects and lattice strain. *J. Mater. Chem. C* **2018**, *6*, 9561−9568.

https://doi.org/10.1021/acs.jpclett.3c01784
J. Phys. Chem. Lett. 2023, 14, 7618−7625